IJP: Drugs and Drug Resistance 13 (2020) 38–50

Contents lists available at ScienceDirect

IJP: Drugs and Drug Resistance

journal homepage: www.elsevier.com/locate/ijpddr

Cholinergic receptors on intestine cells of *Ascaris suum* and activation of nAChRs by levamisole

Mark McHugh[a], Paul Williams[b], Saurabh Verma[b], Jo Anne Powell-Coffman[a], Alan P. Robertson[b], Richard J. Martin[b,*]

[a] Department of Genetics, Development and Cell Biology, Iowa State University, Ames, IA, USA
[b] Department of Biomedical Sciences, College of Veterinary Medicine, Iowa State University, Ames, IA, USA

ARTICLE INFO

Keywords:
Levamisole
Nicotinic acetylcholine receptors
Intestine
Calcium signaling

ABSTRACT

Cholinergic agonists, like levamisole, are a major class of anthelmintic drugs that are known to act selectively on nicotinic acetylcholine receptors (nAChRs) on the somatic muscle and nerves of nematode parasites to produce their contraction and spastic paralysis. Previous studies have suggested that in addition to the nAChRs found on muscle and nerves, there are nAChRs on non-excitable tissues of nematode parasites. We looked for evidence of nAChRs expression in the cells of the intestine of the large pig nematode, *Ascaris suum,* using RT-PCR and RNAscope *in situ* hybridization and detected mRNA of nAChR subunits in the cells. These subunits include components of the putative levamisole receptor in *A. suum* muscle: *Asu-unc-38, Asu-unc-29, Asu-unc-63* and *Asu-acr-8*. Relative expression of these mRNAs in *A. suum* intestine was quantified by qPCR. We also looked for and found expression of G protein-linked acetylcholine receptors (*Asu-gar-1*). We used Fluo-3 AM to detect intracellular calcium changes in response to receptor activation by acetylcholine (as a non-selective agonist) and levamisole (as an L-type nAChR agonist) to look for evidence of functioning nAChRs in the intestine. We found that both acetylcholine and levamisole elicited increases in intracellular calcium but their signal profiles in isolated intestinal tissues were different, suggesting activation of different receptor sets. The levamisole responses were blocked by mecamylamine, a nicotinic receptor antagonist in *A. suum,* indicating the activation of intestinal nAChRs rather than G protein-linked acetylcholine receptors (GARs) by levamisole. The detection of nAChRs in cells of the intestine, in addition to those on muscles and nerves, reveals another site of action of the cholinergic anthelmintics and a site that may contribute to the synergistic interactions of cholinergic anthelmintics with other anthelmintics that affect the intestine (Cry5B).

1. Introduction

Parasitic infections by soil-transmitted helminths (STHs: *Ascaris*, *Trichuris* and hookworm) are a major medical and public health concern in many developing countries. The frequency of these infections is staggering, with estimates of approximately 1.5 billion humans being infected globally (WHO, 2017); over the world, the high morbidity reduces worker productivity by 6.3 million Disability Adjusted Life Years (DALYs) per year. Poverty is correlated with the levels of these infections that degrades worker health, worker output and school performance in children. There is also impairment of the immune system, leading to exacerbation of HIV/AIDS and increased susceptibility to other illnesses such as tuberculosis and malaria (Fincham et al., 2003; Le Hesran et al., 2004; Brooker et al., 2007; Alexander and De, 2009). In livestock, STHs cause lost food production and reduced economic returns that contribute further to poverty (De Silva et al., 2003; Puttachary et al., 2013).

In the absence of adequate sanitation and effective vaccines, control of these infections relies on three major classes of anthelmintic drugs: benzimidazoles like albendazole, the macrocyclic lactones like ivermectin, and the nicotinic cholinergics like levamisole and pyrantel. Pyrantel and levamisole act as agonists that selectively gate nicotinic acetylcholine receptor (nAChR) channels on muscle cells of the parasite (Martin and Robertson, 2010; Abongwa et al., 2017). Opening of

Abbreviations: nAChR, nicotinic acetylcholine receptor; GARs, G protein-linked acetylcholine receptors; STH, Soil-Transmitted Helminth; DALYs, Disability Adjusted Life Years; qPCR, quantitative real-time polymerase chain reaction; RT-PCR, reverse transcription polymerase chain reaction; *Asu*, *Ascaris suum*; APF, *Ascaris* Perienteric Fluid; ARS, *Ascaris* Ringers Solution; FFPE, Formalin-Fixed Paraffin-Embedded; PBS, phosphate buffered saline; NBF, neutral-buffered formalin

* Corresponding author. 2018 College of Vet Med, 1800 Christensen Dr, Ames, IA, 50011, USA.
E-mail address: rjmartin@iastate.edu (R.J. Martin).

https://doi.org/10.1016/j.ijpddr.2020.04.002
Received 21 December 2019; Received in revised form 13 April 2020; Accepted 14 April 2020
Available online 25 April 2020

muscle nAChRs produces depolarization, spastic paralysis and consequent expulsion of the parasite from the host (Aubry et al., 1970; Aceves et al., 1970; Martin and Robertson, 2007). Frequent use of these anthelmintics has led to the emergence of widespread drug resistance in animal parasites (Prichard, 1994) and there is concern about the development of resistance in human parasites. The limited number of anthelmintic drugs and the development of resistance drives the need to determine how existing anthelmintic act, to understand and control resistance and develop novel drugs and combinations.

nAChRs, the target sites of cholinergic anthelmintics, are pentameric membrane proteins comprised of five subunits that surround a central cation-permeable pore (Devillers-Thiery et al., 1993; Unwin, 1993). Combinations of different nAChR subunits leads to the formation of heteromeric receptors on muscle cells that give rise to a diversity of receptor subtypes, each with different pharmacology and anthelmintic sensitivities (Williamson et al., 2009; Buxton et al., 2014; Verma et al., 2017). In vertebrates and the parasitic nematode *Brugia malayi*, nAChR subunit expression has been shown to be in both excitable cells, like nerve and muscle, and in non-excitable cells. Examples of nAChRs on non-excitable cells in mammals include: human skin keratinocytes (Grando et al., 1995), human bronchial epithelial and endothelial cells (Wang et al., 2001), human vascular endothelial cells (Macklin et al., 1998), mouse intestine and intestinal crypt-villus organoids that lack nerve (Takashi et al., 2018). In *Brugia malayi,* the presence of nAChR message has been reported in the developing embryo and spermatozoa (Li et al., 2015) but physiological evidence of activation of nAChRs in non-excitable cells in nematodes is lacking.

Of particular interest to us here, is the presence of functioning nAChRs on cells other than muscles and nerves. These paracrine nAChRs on non-excitable cells in nematode parasites may be activated by cholinergic anthelmintics and play a role in their effects on the parasites. This interest was provoked by the potentiating effect of cholinergic anthelmintics on the action of Cry5B, a pore-forming peptide Bt toxin that acts on the intestinal tract of nematodes (Hu et al., 2010, 2018). These observations suggest the presence of nAChRs within the intestine that are also the site of action of the cholinergic anthelmintics and that a combination of Cry5B and cholinergic anthelmintics could be advantageous.

In this paper we explore the presence of nAChRs in the nematode intestine. The nematode intestine is important for enzymatic digestion and nutrient absorption (McGhee et al., 2007; Yin et al., 2008). In addition, other processes such as ion transport (Nehrke, 2003), defense against environmental toxins (Park et al., 2001; Rosa et al., 2015) and innate immunity to microbial infection (Rosa et al., 2015; Schulenburg et al., 2004) are present in the intestine of nematodes.

We used *Ascaris suum* for our studies (Martin, 1993). This parasite is closely related to *Ascaris lumbricoides* seen in humans (Boes and Helwigh, 2000; Nejsum et al., 2005). We used RT-PCR, quantitative Real-time PCR (qPCR), and RNAscope to identify and quantify, in the muscle and intestine of adult female *A. suum,* the relative expression of the nAChR subunits that constitute the putative levamisole receptor, namely: *Asu-unc-38, Asu-unc-29, Asu-unc-63* and *Asu-acr-8*. RNAscope is an *in-situ* hybridization technique that uses a novel signal amplification method that allows for the detection, visualization and localization of target RNAs as punctate dots in individual cells (Wang et al., 2012; Anderson et al., 2016). Our observations indicate the presence of nAChRs in the intestine. Furthermore, we used calcium imaging to show that application of acetylcholine and levamisole to the intestine transiently increases cytoplasmic calcium. Our findings revealed evidence of functioning nAChRs in the intestine that may be exploited further by existing cholinergic anthelmintics or novel therapeutic combinations.

2. Materials and methods

2.1. Collection and maintenance of A. suum worms

Adult female *A. suum* worms were collected from the JBS Swift and Co. pork processing plant at Marshalltown, Iowa. Worms were maintained in *Ascaris* Ringers Solution (ARS: 13 mM NaCl, 9 mM $CaCl_2$, 7 mM $MgCl_2$, 12 mM $C_4H_{11}NO_3$/Tris, 99 mM $NaC_2H_3O_2$, 19 mM KCl and 5 mM glucose pH 7.8) at 32 °C for 24 h to allow for acclimatization prior to use in experiments. The worms were used the next day for experiments.

2.2. Histological preparation of A. suum

For histological analysis of the morphology of *A. suum*, 1 cm of an adult female worm was cut transversely, ~3 cm caudal to the pharyngeal region. Subsequently, the sample was washed in phosphate buffered saline (PBS) and immediately fixed in 10% neutral-buffered formalin for 24 h at room temperature. The fixed sample was dehydrated and infiltrated with paraffin, followed by manual embedding into paraffin wax blocks. Tissue sections of 5 μm thickness were made using a microtome after hardening of the paraffin wax mold, and subsequently mounted on Superfrost® Plus microscope slides (Fisher Scientific Pittsburgh, PA, USA). The section was subjected to hematoxylin and eosin staining and observed with an Olympus BX53 Microscope® (Olympus America, Inc., Center Valley, PA, USA), equipped with an Olympus DP73 (Olympus America, Inc., Center Valley, PA, USA) camera which was used for capturing images using the cellSens™ Imaging Software version 1.12 (Olympus Corporation of the Americas, Waltham, MA, USA).

2.3. Intestinal tissue and muscle bag preparation

Dissection was conducted on adult *A. suum* females (n = 5) by cutting a 2 cm section from the anterior region of the worm, ~3 cm caudal to the pharyngeal region. The resulting section was cut along one of the lateral lines and pinned cuticle side down onto a 35 × 10 mm Petri-dish lined with Sylgard, to form a muscle flap, thus exposing the intestine and muscle bags. The intestine was gently removed using fine forceps. Next, the body wall flap with exposed muscle bags was washed with autoclaved *Ascaris* perienteric fluid (APF: 23 mM NaCl, 110 mM Na acetate, 24 mM KCl, 6 mM $CaCl_2$, 5 mM $MgCl_2$, 11 mM glucose, 5 mM HEPES, pH 7.6) to remove fragments of the intestine. The APF solution was then replaced with collagenase solution for a period of 5 min at room temperature to facilitate the separation of muscle bags from the body wall of the worm. After collagenase treatment, the muscle flap was washed with APF, and muscle bags were separated from the body wall with fine forceps, and collected with a micropipette. Both intestine and muscle bag tissue were immediately snap-frozen in liquid nitrogen and stored at – 80 °C until further use.

2.4. A. suum cDNA synthesis and RT-PCR detection of nAChR subunits

Muscle bags and intestinal tissue of *A. suum* were homogenized separately in 1 ml of Trizol reagent using a mortar and pestle, followed by total RNA extraction according to the Trizol Reagent protocol (Invitrogen/Life Technologies, Carlsbad, CA, USA). One microgram (1 μg) of total RNA from each tissue was treated with DNase I (Quanta Biosciences, Inc., Gaithersburg, MD, USA) for the removal of residual genomic DNA. This was followed by reverse transcription (RT) using qScript™ Flex cDNA Synthesis kit (Quanta Biosciences, Inc., Gaithersburg, MD, USA) following the manufacturer's protocol. PCR

was conducted to detect the presence of *Asu-unc-38* (EU053155.1), *Asu-unc-63* (KY654348.1), *Asu-unc-29* (EU006073.1) and *Asu-acr-8* (KY654347.1) using primers that were designed for targeting transmembrane 1 to transmembrane 4 (TM1-TM4) regions of each gene. *Asu-gapdh* (AB058666.1) was used as a reference gene. We also looked for expression of the G protein-linked acetylcholine receptor, *Asu-gar-1* (FJ609743.1) in the intestine of adult female worms. *Asu-gar-1* is alternatively spliced with two isoforms: *Asu-gar-1a* (1956 bp) and *Asu-gar-1b* (1875 bp). We aligned the nucleotide sequences of both isoforms a and b using the Clustal Omega multiple sequence alignment tool and designed receptor-specific primers targeting the end of transmembrane 2 and downstream transmembrane 5 where both isoforms had 100% similarity. Again, *Asu-gapdh* was used as a reference gene. The primers used for each geneare presented in Table S1. The cycling conditions for PCR were an initial denaturation for 2 min at 95 °C, followed by 35 cycles of 95 °C for 30 s, 54 °C for 35 s, 72 °C for 45 s, and a final extension at 72 °C for 5 min. PCR products were then separated on a 1% Agarose ethidium bromide gel, followed by visualization and sequencing to confirm the identity of the subunits.

2.5. Analysis of mRNA levels by quantitative real-time PCR

To quantify the relative mRNA transcript levels of each subunit in the intestine and muscle bags, cDNA was synthesized from 1 μg of three adult female *A. suum* total RNA samples (n = 3) that were extracted for use in PCR experiments. Quantification standards were generated by pooling equal volumes of cDNA from each worm sample followed by serial dilutions. Target genes with fragments ranging from 150 to 200 bp between TM3 and TM4 regions were amplified by qPCR from each cDNA sample. This was also done for the reference gene *Asu-gapdh*. All primers for qPCR are presented in Table S2. The real-time PCR reaction mixture consisted of 1 μl of cDNA template, 1 μl of primer mix (500 nM [each]), and 10 μl of SsoAdvanced™ Universal SYBR® Green Supermix (Bio-Rad), with the final volume made up to 20 μl with Nuclease-free water. The cycling conditions included an initial denaturation for 30 s at 95 °C, 40 cycles of 95 °C for 15 s, 54 °C for 20 s, 65 °C for 5 s and a final melting curve step. Cycling was performed using a CFX 96 real-time system (Bio-Rad, Hercules, CA) and transcript quantities were derived by the system software, using the generated standard curves. mRNA expression levels for each subunit (*Asu-unc-38, Asu-unc-29, Asu-unc-63* and *Asu-acr-8*) was estimated relative to the reference gene (*Asu-gapdh*) using the Pfaffl Method. The qPCR experiments were repeated 3 times for each gene (all subunit mRNA quantifications were performed in triplicate for each worm's muscle bag sample and intestinal tissue sample: 3 biological replicates each with 3 technical replicates). Statistical analysis was done using the one-way analysis of variance (ANOVA), $P < 0.05$ with GraphPad Prism 5.0 (Graphpad Software, Inc., La Jolla, CA, USA). The data are presented as relative expression levels in mean ± SEM X1000 units for each nAChR subunit relative to *Asu-gapdh* in muscle bags and intestinal tissue. Comparisons were made using Tukey's post-hoc test.

2.6. Preparation of formalin-fixed paraffin-embedded (FFPE) tissue for RNAscope ISH

Cross sectional dissections of 1 cm was made from adult female *A. suum* worms (n = 3) ~4 cm below the pharyngeal region. Each dissected worm sample was immediately placed in fresh 10% neutral-buffered formalin (NBF) for 24 h at room temperature, followed by dehydration with paraffin, and manual embedding into paraffin wax blocks. Tissue sections of 5 μm thickness were then made using a microtome, and subsequently mounted on Superfrost® Plus slides (Fisher Scientific Pittsburgh, PA, USA).

2.7. RNAscope in situ hybridization assay

RNAscope *in situ* hybridization (RNAscope ISH) was conducted on FFPE tissue sections using the RNAscope® 2.0 HD Assay (Advanced Cell Diagnostics Inc., Hayward, CA, USA) according to the manufacturer's instructions. FFPE tissue section slides were deparaffinized by incubating for 60 min at 60 °C, followed by submersion in xylene for 5 min, incubation in 100% ethanol for 1 min and then air dried. Subsequently, each section was pre-treated for cell permeabilization and target RNA access, using the RNAscope pretreatment reagents. The individual target probes *Asu-unc-38* (Catalog # 480941), *Asu-unc-29* (Catalog #480931), *Asu-acr-8* (Catalog # 549511) *and Asu-unc-63* (Catalog # 480951) along with negative (*dapB*, targets bacterial gene) and positive (*Asu-gapdh*) control probes were then hybridized for 2 h at 40 °C, followed by RNAscope amplification, using several hybridization buffers (Amp 1–6). Subsequently, each slide was washed with wash buffer for 2 min at room temperature. Fast red detection was performed, followed by DAB chromogenic detection and counterstaining with hematoxylin. Stained slides were examined with an Olympus BX53 Microscope® (Olympus America, Inc., Center Valley, PA) with pink punctate dots representing positive expression of mRNA transcript for each subunit. All probes were designed and synthesized by Advanced Cell Diagnostics.

2.8. Subcellular quantification of mRNA punctate dot analysis

After the RNAscope ISH assay, mRNA transcript (pink punctate microdots) abundance for each of the investigated subunits was quantified across all intestinal tissue visible in the cross sections and cell regions divided into basolateral, nuclear, peri-nuclear, central and apical areas for each of the intestines of three worms (n = 3), Fig. 4A. The data were expressed as mean density of mRNA transcripts/μm^2. We also quantified the density of the subunit mRNAs dots in the basolateral (B) or central (C) regions of the columnar intestinal cells, Fig. 4A.

For accurate quantification of punctate dots in the intestine of each worm, the intestine was divided into several photographed frames with each image captured at 200× magnification. These frames covered an area of the intestine of ~10,000 μm^2. Each cross-sectional slide of the worms was viewed with an Olympus BX53 Microscope® (Olympus America, Inc., Center Valley, PA, USA), equipped with an Olympus DP73 camera (Olympus America, Inc., Center Valley, PA, USA) that was connected to the microscope. The camera and microscope were connected to a computer where images were transferred and displayed using the cellSens™ Imaging Software version 1.12 (Olympus Corporation of the Americas, Waltham, MA, USA). Caution was taken not to capture overlapping regions. The total area of the intestinal sections in each frame was acquired using the Halo™ Image Analysis Software version 2.0.1145.19 (Indica Labs, Corrales, NM, USA). Each image frame was then analyzed manually to count the number of punctate dots for the subunits using the Windows 10 Paint Desktop App.

The total number of dots were tabulated for each frame and cell region . To calculate the density of each subunit distribution in the intestine cells, the total number of punctate dots in each frame was divided by the measured area of the intestine (μm^2). The data was analyzed using GraphPad Prism 5.0 (Graphpad Software Inc., La Jolla, CA, USA). We used one-way ANOVA followed by the Tukey multiple comparison test, to determine statistical differences ($P < 0.05$) between the densities of the subunits for each intestinal cell region. Results were displayed as mean ± SEM.

2.9. Intestinal calcium imaging

A 2 cm section of intestine was collected as described earlier with fine forceps and cut open to make a flap. Subsequently, the intestinal

flap was placed onto a coverslip (24 × 50 mm) and pinned using a slice anchor (26 × 1 mm × 1.5 mm grid, Warner Instruments, Hamden, CT), immersed in *Ascaris* Perienteric Fluid with no added $CaCl_2$ in a laminar flow chamber (Warner RC26G, Warner Instruments, Hamden, CT). The calcium concentration of APF with no added $CaCl_2$ was measured and found to be < 100 μM. Fluo-3AM loading was achieved by incubating the intestine in APF solution with no added $CaCl_2$ containing 5 μM Fluo-3AM and 10% Pluronic F-127 (10% v/v) for 1 h with the chamber connected to a Dual Automatic Temperature Controller (Warner Instruments, Hamden, CT). The chamber temperature was maintained between 34 and 36 °C to allow cleavage of the ester group by endogenous non-specific esterases. After 1 h, the excess Fluo-3AM solution was discarded, and the sample was incubated in APF containing 500 μM $CaCl_2$ for an additional 15 min at 34–36 °C to promote Ca^{2+} loading into the intestinal cells. All incubations were done in the absence of light to prevent degradation of the fluorescent dye. After incubation the sample was continuously perfused with APF containing 500 μM $CaCl_2$. All solutions were delivered to the chamber under gravity feed through solenoid valves controlled using a VC-6 six channel Valve Controller (Warner Instruments, Hamden, CT) through an inline heater set at 37 °C (Warner Instruments, Hamden, CT) at a rate of 1.5 mL/min.

At the start of all experiments, samples were exposed to APF containing 500 μM $CaCl_2$ wash under blue light for a minimum of 3 min to promote settling and equilibration of the fluorescent signal and to monitor for any spontaneous Ca^{2+} signaling. Intestinal tissues were then bathed in 30 μM acetylcholine, or 30 μM levamisole, or 30 μM acetylcholine followed by 30 μM levamisole after a 5 min wash after a drug application. For the antagonist experiment, samples were exposed to either 10 μM mecamylamine (antagonist) alone, a combination of 10 μM mecamylamine and 30 μM levamisole or 30 μM levamisole followed by a combination of 10 μM mecamylamine and 30 μM levamisole if an increase in Ca^{2+} was observed. 30 μM acetylcholine, 30 μM levamisole and 10 μM mecamylamine applications were made within APF containing 500 μM $CaCl_2$. All samples were then tested with 10 mM $CaCl_2$ after drug applications as a positive control and for response amplitude comparisons. For 10 mM $CaCl_2$ a total of 689 regional measurements were obtained from 12 intestinal preparations (n = 6 adult female worms). For acetylcholine, 280 regional measurements were analyzed from 7 intestinal preparations (n = 4 adult female worms) and for levamisole, a total of 241 regional measurements were analyzed from 5 intestinal preparations (n = 4 adult female worms). Mecamylamine had 300 regional measurements from 5 intestinal preparations (n = 3 adult female worms) and levamisole + mecamylamine had 230 recordings from 4 intestinal preparations (n = 4 adult females). A region consisted of a square area of 50 μm × 50 μm of adjacent cells.

All recordings were performed on a Nikon Eclipse TE3000 microscope (20X/0.45 Nikon PlanFluor objective), fitted with a Photometrics Retiga R1 Camera (Surrey, BC, Canada). Light control was achieved using a Lambda 10–2 two filter wheel system with shutter controller (Lambda Instruments, Switzerland). Filter wheel one was set on a green filter between the microscope and camera. Filter wheel two was set on the blue filter between a Lambda LS Xenon bulb light box which delivered light via a fiber optic cable to the microscope (Lambada Instruments, Switzerland). Blue light emission was controlled by using a shutter. Minimal illumination exposure was used to prevent photo bleaching.

All Ca^{2+} signal recordings were acquired and analyzed using MetaFluor 7.10.2 (MDS Analytical Technologies, Sunnyvale, CA) with exposure settings at 250 ms with 2x binning. Maximal Ca^{2+} signal amplitudes (ΔF) were calculated using the equation F1–F0/F0 x 100, where F1 is the fluorescent value and F0 is the baseline value. All F0 values were determined as being the value at the time any stimulus was applied to the sample for all traces analyzed. All pictures were taken using Occular 2.0.1.496 (Digital optics, Auckland, New Zealand).

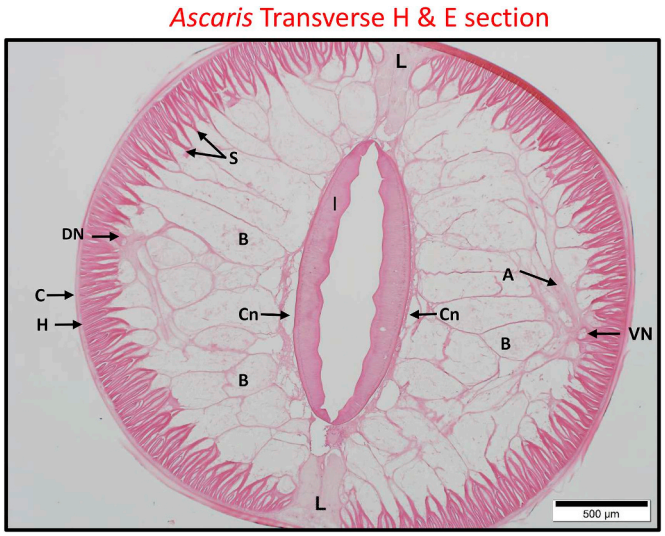

Fig. 1. Hematoxylin and Eosin stained transverse section through *Ascaris suum* showing various regions: the cuticle (C); hypodermis (H); lateral lines (L); contractile spindles (S); arms (A) dorsal nerve cord (DN); ventral nerve cord (VN); muscle bags (B); Canals containing perienteric fluid (Cn) and intestine (I).

Exposure settings were 150 ms with 2x binning. Statistical analysis was performed using two-tailed unpaired student *t*-tests in GraphPad Prism 5.0 (Graphpad Software, Inc., La Jolla, CA, USA).

3. Results

3.1. Transverse section of Ascaris suum

Fig. 1 shows a hematoxylin and eosin stained transverse section through an *Ascaris suum* female worm, 1 cm anterior to the vulva. The section shows the cuticle (C) that surrounds the worm, beneath which lies the hypodermis (H). The muscle tissue includes the contractile spindles (S) and arms (A) that connect the spindles to the nerve cords and the bag region (B). The dorsal and ventral halves of the animal are separated by two lateral lines (L), and the intestine (I). Canals (Cn) that form the perienteric space are found between the intestine and bag regions of the muscle cells; they provide a mechanism for fluid transport along the parasite. In addition, nutrients may be absorbed from the intestine and then moved, through the perienteric canals (Cn). The muscle cells are innervated by excitatory or inhibitor motor neurons of the dorsal (DN) or ventral (VN) nerve cords that are at the end of the arms.

3.2. nAChR subunit mRNA expression in A. suum muscle and intestinal cells

Rosa et al. (2014) used RNA-seq to indicate the presence of nAChR subunit message in the intestine of *A. suum*. We isolated mRNA from explanted intestine and muscle tissue from 5 individual adult *Ascaris* and used RT-PCR to identify the presence of specific nAChR subunits. We looked for and detected expression of *Asu-unc-29, Asu-unc-63, Asu-unc-38* and *Asu-acr-8*, in both intestinal cells and muscle bags. These data are shown in Fig. 2. The brightest bands in intestine cells were *Asu-unc-38* and *Asu-acr-8*; *Asu-unc-29* bands were in contrast fainter than the others.

3.3. Differential expression of nAChR subunits in muscle bags and intestinal tissue

Expression of the putative L-type nAChR subunits in the muscle bag regions and the intestinal tissue prompted us to measure the relative

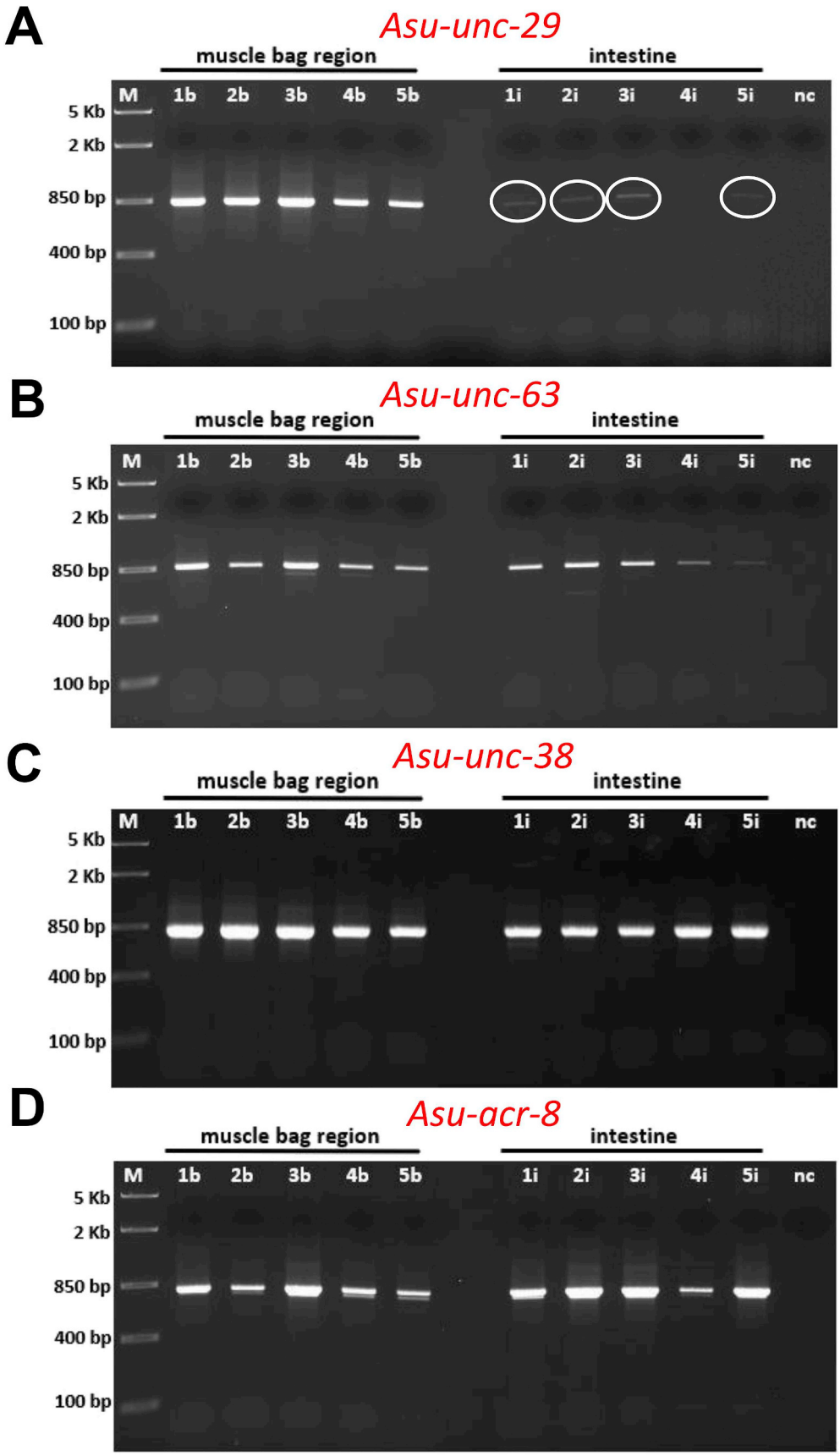

Fig. 2. Localization of nAChR subunits in the muscle bag region and intestine of *A. suum*. RT-PCR analysis of muscle bag (1b, 2b, 3b, 4b, 5b) and intestine (1i, 2i, 3i, 4i, 5i) of five separate adult female *A. suum* worms. Each lane represents an individual worm that muscle bags and intestinal tissue was taken for analysis. M = FastRuler Middle Range DNA Ladder (Thermo Fisher Scientific) and n.c = negative control. (A) *Asu-unc-29* (B) *Asu-unc-63* (C) *Asu-unc-38* (D) *Asu-acr-8*. Note the reduced intensity of the bands (encircled white) with *Asu-unc-29* (A) from the intestine.

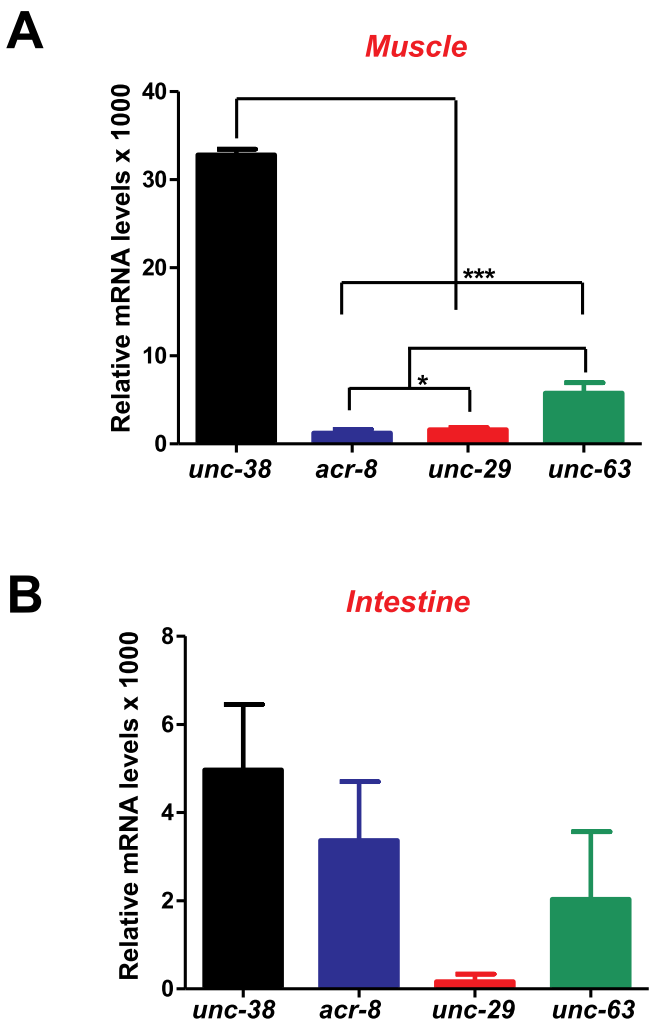

Fig. 3. Differential expression of nAChR subunits in muscle and intestine of *Ascaris suum*. Bar charts (expressed as mean ± SEM) demonstrating qPCR experiments of the relative mRNA levels of *Asu-unc-38* (black bar), *Asu-acr-8* (blue bar), *Asu-unc-29* (red bar) and *Asu-unc-63* (green bar) in: (A) muscle bag region (n = 3 individual worms) and (B) intestinal tissue (n = 3 individual worms) of *A. suum*. qPCR experiments were repeated three times for each gene: 3 biological replicates each with 3 technical replicates. For muscle bags, analysis revealed that *Asu-unc-38* (32.83 ± 0.62) had the highest relative mRNA levels than *Asu-acr-8* (1.23 ± 0.41), *Asu-unc-29* (1.63 ± 0.22, n = 3) and *Asu-unc-63* (5.77 ± 1.19); *** $P < 0.001$. *Asu-unc*-63 had higher mRNA levels of expression than *Asu-acr-8* and *Asu-unc-29*; * $P < 0.05$. The means for the mRNA expression of the intestinal were lower but showed similar trends with *Asu-unc-38* (4.97 ± 1.49) being the highest, followed by *Asu-acr-8* (3.37 ± 1.34), *Asu-unc-29* (0.17 ± 0.17) and *Asu-unc-63* (2.03 ± 1.53) but the differences did not reach statistical significance ($P = 0.1250$; $n=3$ *for all subunit genes*). (For interpretation of the references to colour in this figure legend, the reader is referred to the Web version of this article.)

mRNA expression levels of each subunit to examine the difference. Using qPCR, we compared mRNA expression levels of each subunit in the intestine and muscle bag of the parasite relative to a reference gene, *Asu-gapdh*.

Our analysis of the muscle bag region showed that mean mRNA expression levels for *Asu-unc-38* was 6-fold higher than that of *Asu-unc-63*, and approximately 30 times higher than *Asu-acr-8* and *Asu-unc-29* (Fig. 3A). *Asu-unc*-63 mRNA levels were 5-fold greater than *Asu-unc-29* and 3.5-fold higher than *Asu-acr-8*, Fig. 3A. The much higher expression levels of *Asu-unc-38* is interesting and suggests that it may contribute to more than one type of nAChR.

When we looked at expression levels of mRNA in the intestine, we found them to be much lower than in the muscle, Fig. 3B. The muscle *Asu-unc-38,* for example, was nearly 7x higher than the intestine *Asu-unc-38*. Although the mean mRNA expression levels of intestine *Asu-unc-38* appeared greater than *Asu-acr-8,* which in turn appeared greater than *Asu-unc-29* and *Asu-unc-63*, the sample-to-sample variation was high, lessening confidence that the values are significantly and consistently different. Nonetheless, the presence of mRNA for the subunits of the putative L-type nAChR in the intestine suggests the presence of levamisole receptors there.

3.4. RNAscope reveals heterogeneous subcellular distribution of intestinal nAChR subunit mRNAs

We used RNAscope *in situ* hybridization (ISH) to localize the distribution of nAChR subunit mRNAs within the intestinal cells. Each individual 1–2 μm pink dot, represents an individual RNA molecule and its location within cells. Fig. 4 illustrates representative examples of our RNAscope data.

The intestine is composed of columnar cells that extend from the absorptive brush border on the apical edge, with nuclei located near the basolateral border, Fig. 4A. For RNAscope experiments, we examined transverse histological sections of the intestine for each of the four probes in three individual adult female worms. Fig. 4B shows the results from a *Bacillus* dapB probe, which serves as a negative control; note the absence of any pink punctate dots which would mark mRNA single message strands. Fig. S1 also shows results of *Asu-gapdh* positive control; attention should be drawn to the presence of numerous punctate dots throughout the tissue. The presence of *Asu-unc-29* (Fig. 4C), *Asu-unc-63* (Fig. 4D), *Asu-unc-38* (Fig. 4E) *and Asu-acr-8* (Fig. 4F) *mRNAs* in the columnar cells of the intestine was also seen in all sections examined. Intriguingly, the distribution patterns of the mRNA transcripts for the subunits were heterogeneous. *Asu-unc-29* and *Asu-unc-63* was characterized by sparse distributions of microdots that were more focused in the nuclear and basolateral regions of the intestine, (see arrows: Fig. 4C & D). In contrast, *Asu-unc-38* and *Asu-acr*-8 mRNAs were distributed along the length of the columnar cells (Fig. 4E & F) with a large number of microdots within the central region. These observations from the RNAscope studies, showing the presence of the different nAChR subunit message, coupled with our RT-PCR results, provided further molecular evidence of levamisole-sensitive, L-type nAChRs, in *Ascaris suum* intestinal cells.

3.5. Subcellular distribution of intestinal nAChR subunit mRNAs

The differences in the subcellular localization pattern of each subunit mRNAs in our RNAscope assay led us to quantify those differences. We analyzed the mean density of each subunit mRNA transcripts/μm^2 within the intestinal cells and in the basolateral (B) and central (C) subcellular regions of individual cells where the heterogeneous distribution patterns were observed, Fig. 4A. We found that the mean density of *Asu-unc*-38 mRNA was significantly greater in the columnar cells of the intestine, compared to the mean density of *Asu-unc-29* and *Asu-unc-63;* and the mean density of *Asu-acr-8* was somewhere between that of *Asu-unc-38* and *Asu-unc-29* (Fig. 5A). Results from our quantification of the whole intestine revealed that the RNAscope data was consistent with our earlier qPCR findings. *Asu-unc*-38 mRNAs were more abundant in the intestine, compared to *Asu-unc-29* and *Asu-unc-63*.

RNAscope also revealed a lower density of all subunit mRNAs in the basolateral region of the columnar cells of the intestine compared to the mean distribution throughout the cell, Fig. 5B; but the *Asu-unc-38* transcripts were still the most abundant in the basolateral region when compared to *Asu-acr-8* ($P < 0.05$), *Asu-unc-29* ($P < 0.01$) and *Asu-unc-63* ($P < 0.001$).

The mRNA transcripts for *Asu-unc-38* and *Asu-acr-8* in the central region of the intestine columnar cells were more abundant than the

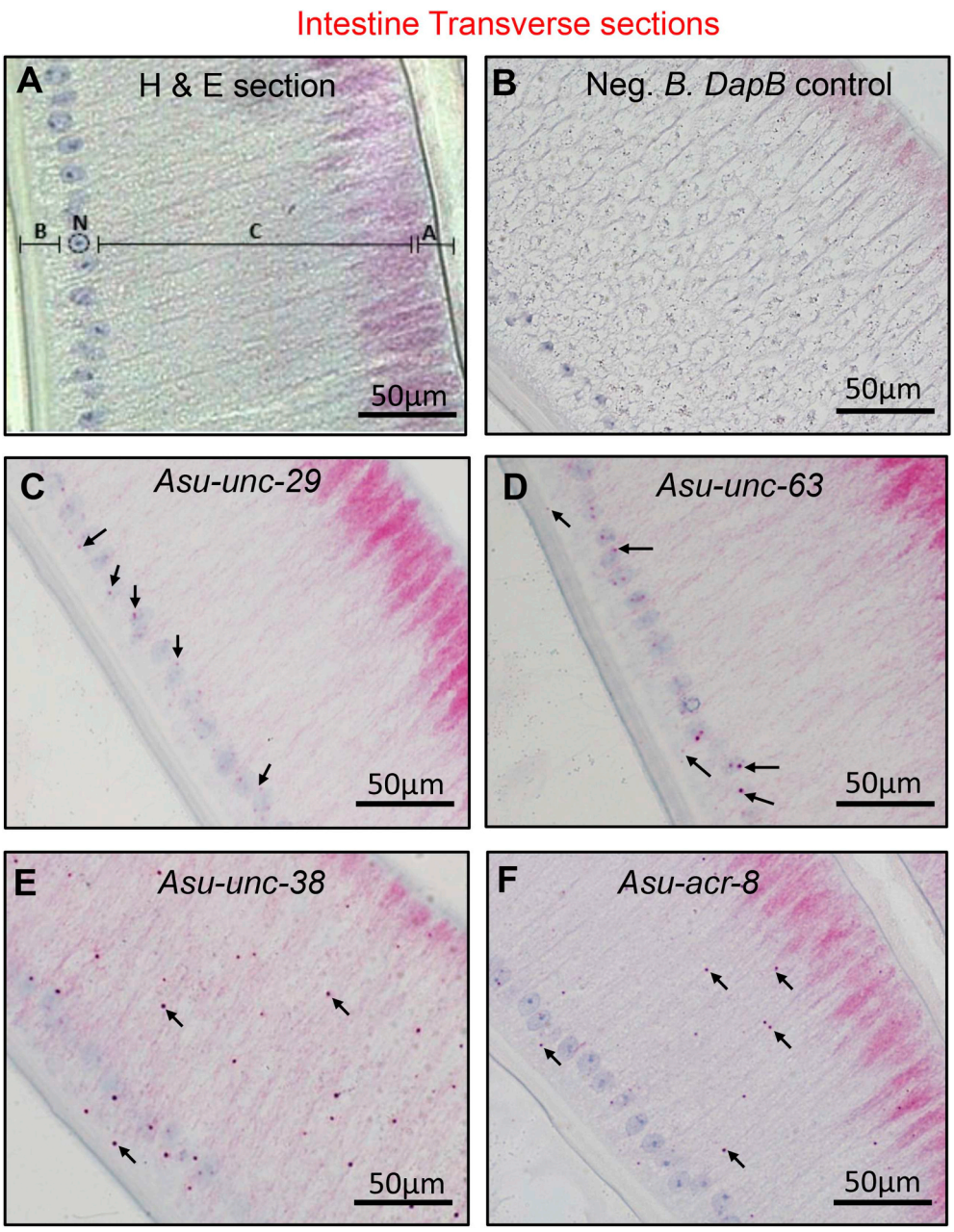

Fig. 4. Subcellular localization of nAChR subunits by RNAscope *in situ* hybridization in *A. suum* intestine. Representative images of *A. suum* intestine. (A) Transverse section of the intestine showing the Basolateral, Nuclear, Central and Apical regions that were observed for nAChR subunit expression. (B) Negative control probe (Bacillus *DapB*) where there are no pink punctate dots. (C) *Asu-unc-29* probe (D) *Asu-unc-63* probe (E) *Asu-unc-38* probe (F) *Asu-acr-8* probe. Pink punctate dots (mRNA transcript) indicate positive signal. Both *Asu-unc-29* and *Asu-unc-63* (C and D) have pink punctate dots within the basolateral region only, while *Asu-unc-38* and *Asu-acr-8* (E and F) have higher abundance of punctate dots distributed throughout all regions of the intestine, specifically the central region. Arrows indicate individual mRNA transcripts (n = 3 worms). (For interpretation of the references to colour in this figure legend, the reader is referred to the Web version of this article.)

transcripts of *Asu-unc-29,* and *Asu-unc-63,* Fig. 5C. Collectively, these findings of subunit mRNA distribution heterogeneity in the basolateral and central regions, suggest different concentrations of nAChR subunits in different regions of the columnar cells and consequently the presence of different nAChR subtypes in different regions of the intestine columnar cells.

3.6. Acetylcholine and levamisole stimulate calcium signals in Ascaris intestine

Having determined that nAChR subunit mRNAs were expressed in the intestine of *Ascaris suum*, we sought evidence of functional responses to acetylcholine and levamisole. To do this we looked for intracellular calcium signals as important markers of activation in the intestinal cells.

To check for the presence of autofluorescence in the intestine, dissected lengths of each worm intestine incubated in Fluo-3AM-free solutions were compared with intestine incubated in 5 µM Fluo-3AM containing 10% Pluronic F-127 (v/v). The micrographs of bright-field (Fig. 6A, left image) and 5 µM Fluo-3AM treated intestinal tissues (Fig. 6A, right image) showed the presence of individual cells as fluorescent spots arranged in groups or tower like microvilli. No equivalent fluorescence of individual cells was observed in the untreated tissue (Fig. 6A, center image). To ensure that changes in Ca^{2+} could be measured in *Ascaris* intestine cells, we applied 10 mM $CaCl_2$. Fig. 6B shows a representative result. Following application of $CaCl_2$, a detectable Ca^{2+} signal was observed that, on average, peaked after 160 ± 1.7 s, with an average increase of 28 ± 0.88% in Fluo-3 fluorescence, which declined shortly after $CaCl_2$ was removed (Fig. 6B and C). We observed no distinct changes in the Ca^{2+} signal in samples

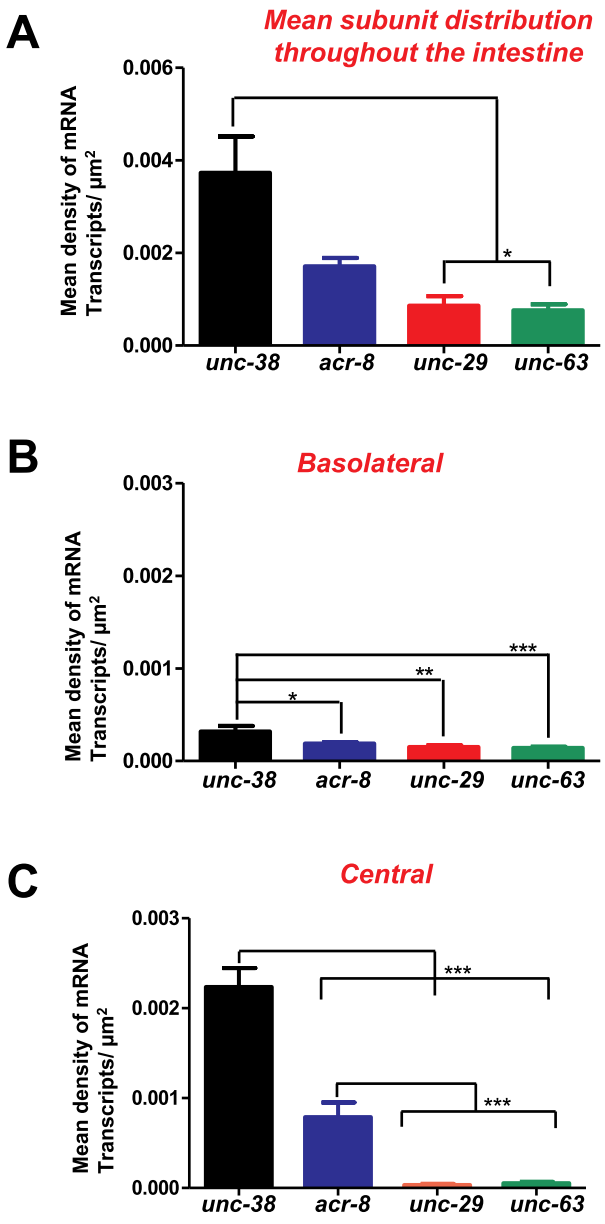

Fig. 5. Quantitative subcellular distribution of nAChR subunit mRNA transcripts in *A. suum* intestine. Bar charts (mean ± SEM) showing the mean density of mRNA transcripts (punctate dots)/µm^2 for *Asu-unc-38*, *Asu-acr-8*, *Asu-unc-29,* and *Asu-unc-63* in various regions of the intestine. A) Mean density of mRNA transcripts for each nAChR subunit in all intestinal tissue visible in the cross section. * Significantly different to *Asu-unc-38* ($P < 0.05$). B) Mean density of mRNA transcripts for each nAChR subunit in basolateral region. * Significantly different to *Asu-unc-38* ($P < 0.05$); **Significantly different to *Asu-unc-38* ($P < 0.01$) and ***Significantly different to *Asu-unc-38* ($P < 0.001$). C) Mean density of mRNA transcripts for each nAChR subunits in the Central region of *A. suum* intestine. *** Significantly different to *Asu-unc-38* or *Asu-acr-8* ($P < 0.001$). *Asu-unc-38* (n = 36 image frames from 3 worms); *Asu-acr-8* (n = 34 image frames from 3 worms); *Asu-unc-29* (n = 39 image frames from 3 worms) and *Asu-unc-63* (n = 39 image frames from 3 worms).

continuously perfused with 500 µM $CaCl_2$ APF (Fig. 6C, APF vs $CaCl_2$).

To measure acetylcholine generated changes in Ca^{2+} signals, we applied 30 µM acetylcholine to the intestine. Acetylcholine (30 µM) generated unique Fluo-3 responses which were typically characterized as a slow and steady rise in Ca^{2+} amplitude, which continued to increase even after removal of acetylcholine (Fig. 6D.) Unlike $CaCl_2$, the acetylcholine responses took significantly longer to reach a peak after application (554 ± 17.49 s) and had a slower decline after peak had been reached (Fig. 6D and F). The overall increases in Fluo-3 fluorescence for acetylcholine were smaller than for the 10 mM $CaCl_2$ test and averaged an increase of 12 ± 0.41% (Fig. 6G). The acetylcholine responses also showed greater fatigue with subsequent applications of acetylcholine being smaller than the first responses.

Acetylcholine is a non-selective cholinergic agonist and can activate a range of acetylcholine receptors including G-protein coupled receptors and different types of nAChRs. As a more selective nicotinic agonists, we applied 30 µM levamisole to Fluo-3AM treated intestines to look for evidence of functional activation of L-type receptors to be indicated by the expression of nAChR subunit message described earlier. Application of levamisole produced a rise in Ca^{2+} amplitude, but generated another distinctive Fluo-3 response profile, which contrasted to that of acetylcholine and $CaCl_2$. Levamisole generated changes in fluorescence took a shorter time to reach peak compared to acetylcholine, averaging at 316 ± 15 s (Fig. 6E and F), but still slower time than 10 mM $CaCl_2$. Additionally, unlike $CaCl_2$ and acetylcholine, the levamisole generated responses declined immediately after reaching peak even when in the continued presence of the stimulus (Fig. 6E). We also quantified the average changes in Fluo-3 intensity; levamisole treatment resulted in significantly smaller increases in fluorescence, 8 ± 0.39%, than acetylcholine, 12 ± 0.41% of (Fig. 6G).

To see if there were differences in the areas of the intestines activated by acetylcholine and levamisole, we calculated the percentage of regions (50 × 50 µm squares) of the intestine that increased in fluorescence following the application of $CaCl_2$, acetylcholine, and levamisole. Fig. 6H, shows that 100% of the regions tested produced responses to $CaCl_2$. Acetylcholine and levamisole also produced responses in 80% and 88% of the regions examined, respectively. There was no significant difference suggesting receptors responding to levamisole (the L-type receptors) and other cholinergic receptors are distributed in a similar way in most of the cells of the intestine.

To verify that the observed calcium signals are a result of manipulation of nAChRs and not through other receptors such as muscarinic G proteins, we PCR screened the intestines of five adult female *A. suum* worms to determine if they express any G protein-linked acetylcholine receptors (GARs). *A. suum* is known to express a GAR protein, *Asu-GAR-1* with an alternatively spliced isoform of the receptor both in the head and tail regions (Kimber et al., 2009). Our RT-PCR results detected that the receptor is expressed in the intestine (Fig. 7A). As mentioned, acetylcholine is a non-selective cholinergic agonist and the observed acetylcholine signal may be partially mediated through GAR-1 as well as nAChRs. To determine if levamisole is signaling solely through nAChRs, we treated intestinal samples with the nicotinic receptor antagonist mecamylamine to block nAChR mediated signaling. First, we exposed tissues to 10 µM mecamylamine and saw no changes in the calcium signal (Fig. 7B and D). Additionally, when 10 µM mecamylamine and 30 µM levamisole were simultaneously applied we also observed no changes in Fluo-3 fluorescence (Fig. 7C and D). Lastly, we applied 30 µM levamisole and upon an increase in the Ca^{2+} signal, we co-applied 10 µM mecamylamine and saw that the signal was terminated, often to a level below the resting level, as the intracellular Ca^{2+} is adjusted by uptake processes (Fig. 7E). These data demonstrate that levamisole stimulates Ca^{2+} signals in the intestine by signaling through nAChRs and not GARs.

4. Discussion

4.1. GAR-1s, nAChRs and a paracrine function

In this study we have observed: message of both nAChR subunits *for Asu-unc-29, Asu-unc-63, Asu-unc-38, Asu-acr-8* and the G protein-linked

acetylcholine receptor (GAR), *Asu-gar-1* in the cells of *A. suum* intestine. We have also observed that acetylcholine and levamisole produced different Ca^{2+} signal profiles indicating that they activate two different sets of receptors. The latency before the beginning of the levamisole calcium response, Fig. 6, was longer but the time to peak was shorter than that of acetylcholine. Acetylcholine is a flexible molecule and a non-selective cholinergic agonist: it can activate a range of acetylcholine receptors including G-protein coupled receptors and different types of nAChRs. Levamisole is a more rigid molecule: it is a selective L-type nAChR agonist in nematodes (Buxton et al., 2014; Verma et al., 2017). Together, these observations indicate the presence and activation of two or more receptor signaling pathways. We interpret these observations to suggest that acetylcholine activates both G-protein acetylcholine receptors (Asu-GAR-1) and nAChRs, and that levamisole activates nAChRs that are blocked by mecamylamine.

Given that nematode intestine cells lack direct innervation, it is

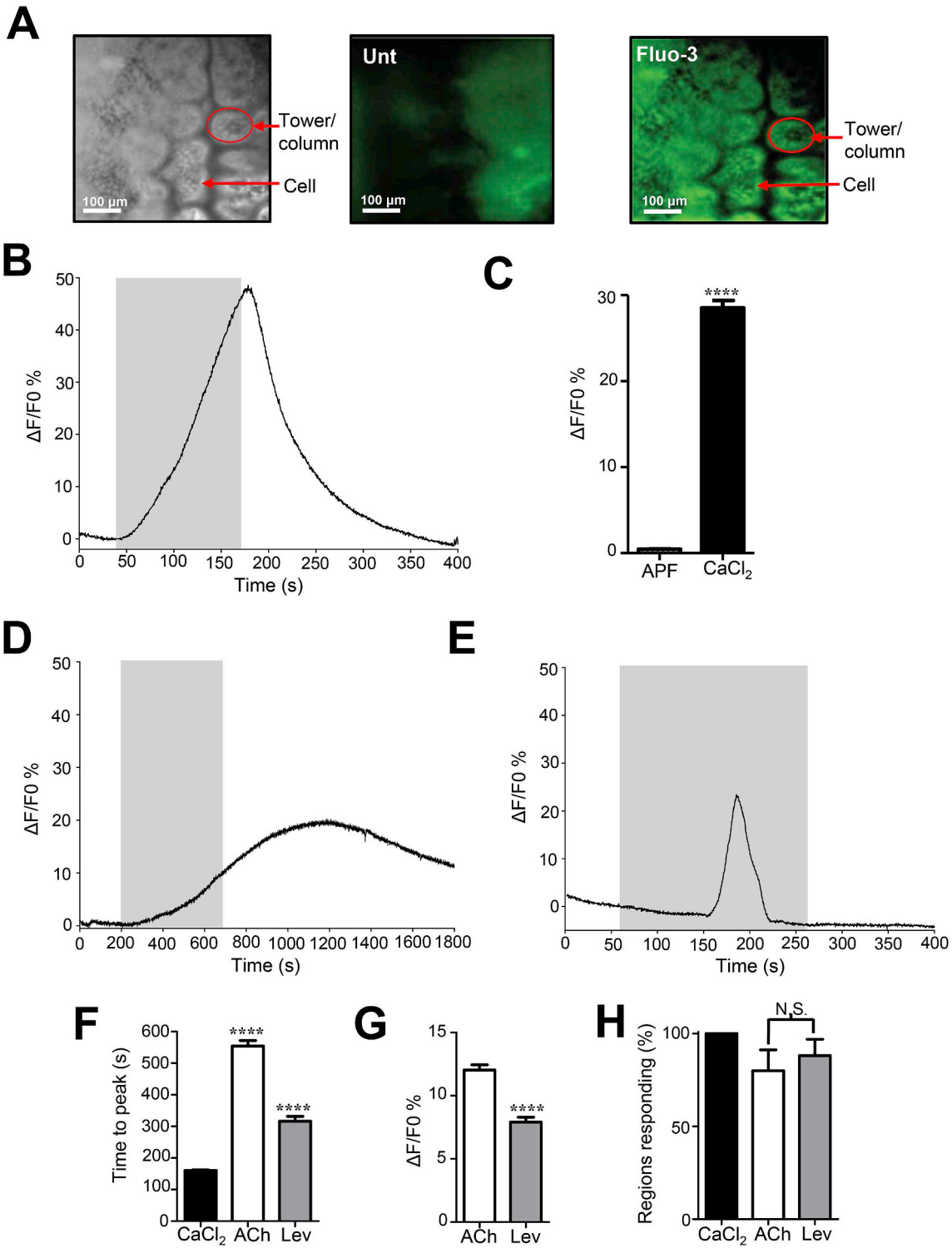

(caption on next page)

Fig. 6. Acetylcholine and levamisole generate Ca^{2+} signals in Fluo-3AM treated *Ascaris* intestines. A) Micrographs of *Ascaris suum* intestinal section under white light (left), untreated fluorescing under blue light (center) and 5 μM Fluo-3AM treated under blue light (right), after 60-min incubation at 35 °C with 10% Pluronic F-127. Key structures, tower/column and cells are highlighted. B) Representative trace of a 10 mM $CaCl_2$ stimulated signal. Grey box indicates application of the stimulus. C) Amplitudes of Ca^{2+} signals in intestines exposed to APF containing 500 μM $CaCl_2$ (untreated) and 10 mM $CaCl_2$ (Black bar). **** Significantly different from 500 μM $CaCl_2$ APF ($P < 0.0001$, t = 18.67, df = 925, unpaired t-test). 500 μM $CaCl_2$ APF $n = 238$ recordings from 8 intestines from 8 individuals; 10 mM $CaCl_2$ $n = 689$ recordings from 12 intestine preparations from 6 individual females. D) Representative trace of a Ca^{2+} signal to 30 μM acetylcholine. Grey box indicates acetylcholine application. E) Representative trace of a Ca^{2+} signal to 30 μM levamisole. Grey box indicates levamisole application. F) Quantification of the time for the Ca^{2+} signal to reach peak after stimulus application for 10 mM $CaCl_2$ (Black bar), 30 μM acetylcholine (White bar) and 30 μM levamisole (Grey bar). **** Significantly different to $CaCl_2$ ($CaCl_2$ vs acetylcholine $P < 0.0001$, t = 33.62, df = 986; $CaCl_2$ vs levamisole $P < 0.0001$, t = 16.15, df = 916, unpaired t-tests). 10 mM $CaCl_2$ $n = 689$ recordings from 12 intestinal preparations from 6 individual females; acetylcholine $n = 280$ recordings 7 intestine from 4 individual worms; levamisole $n = 241$ recordings 5 intestinal preparations from 4 females. G) Amplitudes of Ca^{2+} signals in intestines in response to 30 μM acetylcholine (White bar) and 30 μM levamisole (Grey bar). **** Significantly different to acetylcholine ($P < 0.0001$, t = 7.182, df = 519 unpaired *t*-test). H) Average percentage of recording regions of the intestine with positive increases in Fluo-3 fluorescence to 10 mM $CaCl_2$ (Black bar), 30 μM acetylcholine (White bar) and 30 μM levamisole (Grey bar). N.S. = not significant (acetylcholine vs levamisole $P = 0.6037$, t = 0.5359, df = 10, unpaired *t*-test). All values are represented as means ± SEM. (For interpretation of the references to colour in this figure legend, the reader is referred to the Web version of this article.)

possible that intestinal GAR-1s and nAChRs are involved in a paracrine function, responding to acetylcholine released from adjacent cells. The presence of GARs, nAChRs and acetylcholine synthesis, secretion and degradation is seen in other non-excitable cells such as: human and rat bronchial epithelial cells (Cazzola et al., 2016; Maus et al., 1998); human keratocytes (Slonieka et al., 2015) and skin keratinocytes (Grando et al., 1993, 1995). Mellanby (1955) has detected the presence of acetylcholine in *Ascaris* tissues and Lee (1962) has detected cholinesterase in the intestine and secretions of *Ascaris* intestinal cells. These observations support the hypothesis of a paracrine function for acetylcholine and the receptors we have observed in the intestine. Co-ordination of digestive enzyme secretion and nutrient absorption may be by signaling mediated by GAR-1s and nAChRs of the intestinal cells.

4.1.1. Different distributions of nAChRs subunit message in the basolateral and central regions of the columnar intestine cells

The nAChR subunit message for *Asu-unc-29, Asu-unc-63, Asu-unc-38* and *Asu-acr-8* was found in the somatic muscle and in the intestinal cells of *A. suum*. The protein subunits from this message produce the putative L-subtype levamisole receptor, and in different combinations produce different receptor subtypes (Buxton et al., 2014; Verma et al., 2017). Our quantitative PCR analysis revealed that the subunit mRNA levels were differentially expressed in the muscle bag region and intestinal columnar cells. In addition, RNAscope *in situ* hybridization measurements showed us that the distribution of the message for these subunits was not uniform within the columnar cells of the intestine. The message for *Asu-unc-29, Asu-unc-63, Asu-unc-38* and *Asu-acr-8,* subunits of the putative L-type receptor, had a similar density in the region of the basolateral membrane of the columnar intestinal cells while *Asu-unc-38* and *Asu-acr*-8 had a much higher density than *Asu-unc-29* and *Asu-unc-63* in the central region of the intestinal cells. The relationship between the level of mRNA expression and level of protein expressed in steady-state conditions are usually positively correlated (Liu et al., 2016). If we use this correlation, the different subunit message levels predict that we have combinations of nAChR subunits in the basolateral region of the intestinal cells that contrast with the combinations of the subunits in the central region of the columnar cells. These observations then suggest that there are two or more subtypes of nAChRs involved in activating the columnar intestinal cells: one subtype in the central region with *Asu-unc-38* and *Asu-acr-8* with less or no *Asu-unc-29, Asu-unc-63* subunits; the other subtype with *Asu-unc-38*, *Asu-acr-8, Asu-unc-29* and *Asu-unc-63* subunits like the L-subtype in the basolateral region.

4.1.2. Possible function of the nAChR subtypes located in the basolateral region of the intestinal cells

Given their location, adjacent to the perienteric space, it is possible that basolateral nAChRs are involved in signaling between the muscle bags and the intestine. Acetylcholine released into the perienteric space from the bag regions of the muscle cells or from the intestinal cells can enter the perienteric canals. The perienteric canals can allow distribution of materials (chemicals and nutrients) along the length of the worm. Acetylcholine released into the perienteric space would simultaneously stimulate the L-subtype receptors present on the bag region of *Ascaris* muscle (Qian et al., 2006) and receptors present on the basolateral region of the intestinal cells. The bag region of the muscle is filled with glycogen and takes up nutrients released from the adjacent intestine, requiring coordination between muscle bags and cells of the intestine.

4.1.3. Possible function of the nAChR subtypes located in the central region of the intestinal cells

The location of the nAChR subtypes in the central region of the columnar cells suggests an interaction between adjacent intestinal cells rather than with the muscle cells underneath. These central nAChRs would facilitate a co-ordination of digestive enzyme secretion and nutrient absorption mediated by central region nAChRs of the columnar intestinal cells.

4.1.4. Levamisole and Cry5B

Cry5B is a Cry protein recovered from *Bacillus thuringiensis* that has significant anthelmintic actions. Given the widespread and very effective use of Bt Cry toxins as an insecticide for protection of corn and cotton plants, it is hoped that nematocidal Cry toxins including Cry5B can be developed and used as anthelmintics. Cry5B has potent toxic effects on *C. elegans* and on a range of parasitic nematodes including *Ascaris suum* (Hu et al., 2010, 2018; Urban et al., 2013). The mode of action of Cry5B involves its activation by a gut protease in the nematode, binding to a nematode specific cadherin CDH-8, uptake by intestinal cells dependent on the glycolipid gene *bre-5*, and then a pore-forming process that damages the permeability of the intestine (Peng et al., 2018). Interestingly, nAChR agonists like levamisole and Cry5B have a synergistic anthelmintic action with levamisole increasing the potency of Cry5B (Hu et al., 2010).However, a mechanism for this synergy has yet to be established.

Here we suggest that the action of levamisole on the intestine of the nematode may be to stimulate the digestion processes leading to the release of proteases and activation of Cry5B and its absorption. The activation of digestion by levamisole would then enhance the uptake of nematode intestinal contents, and enhance the internalization of the activated Cry5B, thus facilitating pore formation and the anthelmintic action of Cry5B.

We point out that benzimidazole anthelmintics also have an action on the intestinal cells of *Ascaris* (Borgers and De Nollin, 1975), presumably due to the disruption of microtubulins with binding to β-tubulin (Borgers et al., 1975). Uptake of the benzimidazoles by the nematode parasite is also anticipated to be increased by the cholinergic anthelmintics like levamisole; levamisole is thus predicted to have an additive effect on the anthelmintic action of benzimidazoles.

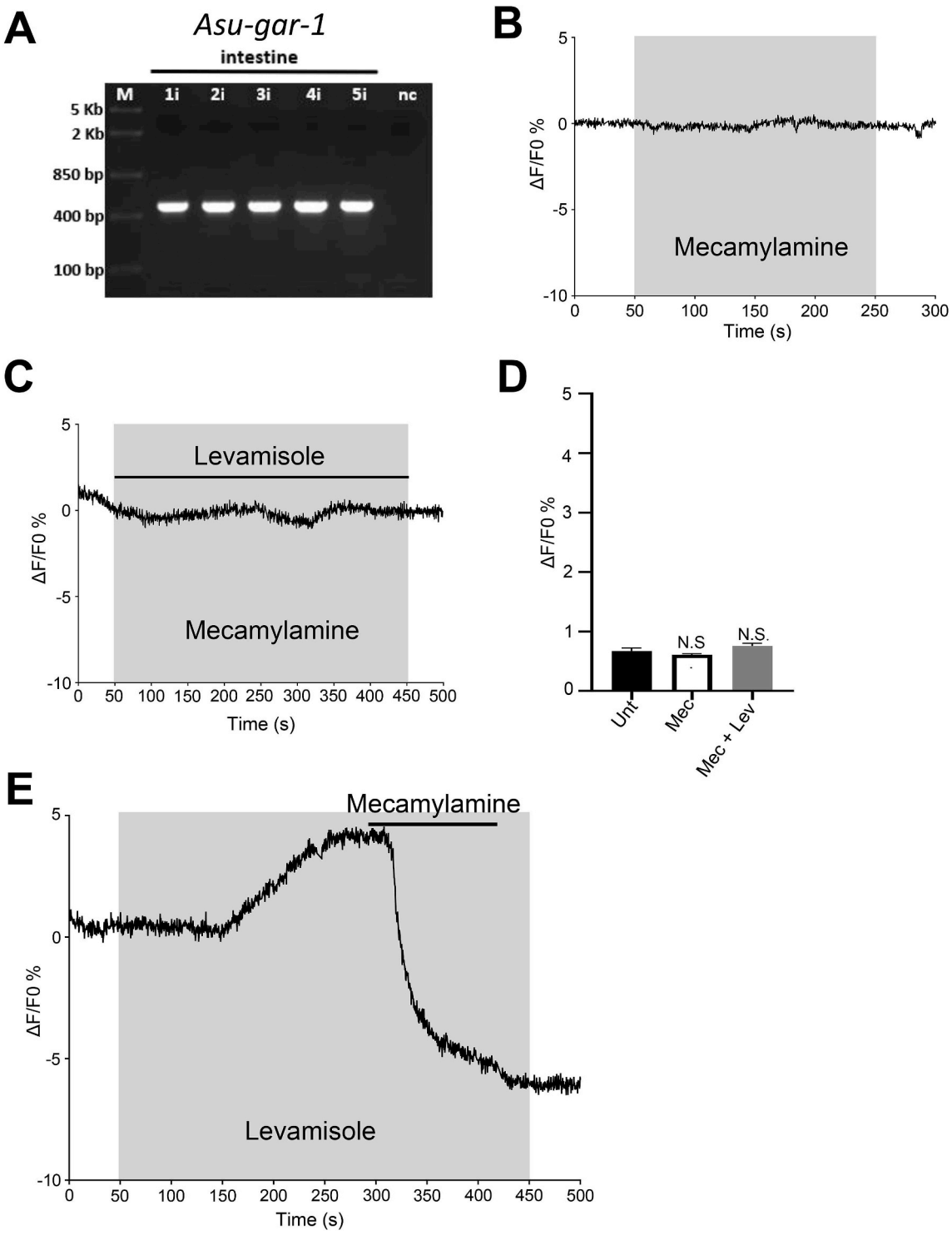

Fig. 7. Intestine *Asu-gar-1* message and mecamylamine inhibition of levamisole mediated Ca^{2+} signals. A) RT-PCR analysis shows the presence of *Asu-gar-1* in the intestine (1i, 2i, 3i, 4i, 5i) of five separate adult female *A. suum*. M = FastRuler Middle Range DNA Ladder (Thermo Fisher Scientific) and n.c = negative control. B) Representative trace to 10 μM mecamylamine. Grey box indicates application of the stimulus. C) Representative trace for simultaneous application of 30 μM levamisole (grey box) and 10 μM mecamylamine (black bar). D) Quantification of maximum changes in Ca^{2+} signal amplitude for untreated (Black bar), 10 μM mecamylamine (White bar) and 30 μM levamisole + 10 μM mecamylamine (Grey bar). N.S. = not significant to untreated (untreated vs mecamylamine $P = 0.2278$, t = 1.207, df = 578; untreated vs levamisole + mecamylamine $P = 0.2365$, t = 1.185, df = 506 unpaired *t*-test). Untreated $n = 280$ recordings from 10 intestinal preparations from 10 individual females; mecamylamine $n = 300$ recordings from 5 intestine taken from 3 individual worms; levamisole + mecamylamine $n = 230$ recordings from 4 intestinal preparations from 4 females. E) Representative trace of the response to 30 μM levamisole before co-application of 10 μM mecamylamine. Grey box indicates levamisole application; black represents mecamylamine. Note that mecamylamine inhibits the response to levamisole and produces a reduction in the Ca^{2+} fluorescence below the resting level due to a delayed uptake process that follows the rise in intracellular Ca^{2+}. All values are represented as means ± SEM.

5. Conclusions

To conclude, we have found evidence that a nematode parasite intestine expresses functioning nAChRs that respond to the cholinergic anthelmintic levamisole. These nAChRs are likely to include different subtypes, some of which may stimulate the processes of digestion and enhance the efficacy of other classes of gut acting anthelmintics.

Declaration of competing interest

The authors declare no conflict of interests.

Acknowledgments

We acknowledge, NIH National Institute of Allergy and Infectious Diseases grants R01AI047194-17 and 5R21AI13967 to RJM, the E. A. Benbrook Foundation for Pathology and Parasitology for support to RJM, NIH R21AI092185-01A1 to APR and the College of Agriculture and Life Sciences for support for MMcH. The funding agencies had no role in the design, execution or publication of this study. The content is solely the responsibility of the authors and does not necessarily represent the official views of the National Institute of Allergy and Infectious Diseases.

Appendix A. Supplementary data

Supplementary data to this article can be found online at https://doi.org/10.1016/j.ijpddr.2020.04.002.

References

Abongwa, A., Martin, R.J., Robertson, A.P., 2017. A Brief Review on the mode of action of antinematodal drugs. Acta Vet. 67, 137–152.
Aceves, J., Erlij, D., Martinez-Maranon, R., 1970. The mechanism of the paralyzing action of tetramisole on Ascaris somatic muscle. Br. J. Pharmacol. 38, 602–607.
Alexander, P.E., De, P., 2009. HIV-1 and intestinal helminth review update: updating a Cochrane Review and building the case for treatment and has the time come to test and treat? Parasite Immunol. 31, 283–286.
Anderson, C.M., Bingqing, Z., Miller, M., Butko, E., Wu, Xingyong, Laver, T., Kernag, C., Kim, J., Luo, Y., Lamparski, H., Park, E., Su, N., Ma, X.J., 2016. Fully automated RNAscope in situ hybridization assays for formalin-fixed paraffin-embedded cells and tissues. J. Cell. Biochem. 117, 2201–2208.
Aubry, M.L., Cowell, P., Davey, M.J., Shevde, S., 1970. Aspects of the pharmacology of a new anthelmintic: pyrantel. Br. J. Pharmacol. 38, 332–344.
Boes, J., Helwigh, A.B., 2000. Animal models of intestinal nematode infections of humans. Parasitology 121, S97–S111.
Borgers, M., De Nollin, S., De Brabander, M., Thienpont, D., 1975. Influence of the anthelmintic mebendazole on microtubles and intracellular organelle movement in nematode intestinal cells. Am. J. Vet. Res. 36, 1153–1166.
Borgers, M., De Nollin, S., 1975. Ultrastructural changes in *Ascaris suum* intestine after mebendazole treatment in vivo. J. Parasitol. 61, 110–122.
Brooker, S., Akhwale, W., Pullan, R., Estambale, B., Clarke, S.E., Snow, R.W., Hotez, P.J., 2007. Epidemiology of plasmodium-helminth co-infection in Africa: populations at risk, potential impact on anemia, and prospects for combining control. Am. J. Trop. Med. Hyg. 77, 88–98.
Buxton, S.K., Charvet, C.L., Neveu, C., Cabaret, J., Cortet, J., Peineau, N., Abongwa, M., Courtot, E., Robertson, A.P., Martin, R.J., 2014. Investigation of acetylcholine receptor diversity in a nematode parasite leads to characterization of tribendimidine- and derquantel sensitive nAChRs. PLoS Pathog. 10 (1), e1003870.
Cazzola, M., Calzetta, L., Puxeddu, E., Ora, J., Facciolo, F., Rogliani, P., Gabriella, M.G., 2016. Pharmacological characterization of the interaction between glycopyrronium bromide and indacaterol fumarate in human isolated bronchi, small airways and bronchial epithelial cells. Respir. Res. 17, 70.
De Silva, N.R., Brooker, S., Hotez, P.J., Montresor, A., Engels, D., Savioli, L., 2003. Soil-transmitted helminth infections: updating the global picture. Trends Parasitol. 19, 547–551.
Devillers-Thiery, A., Galzi, J.L., Eisele, J.L., Bertrand, S., Bertrand, D., Changeux, J.P., 1993. Functional architecture of the nicotinic acetylcholine receptor: a prototype of ligand-gated ion channels. J. Membr. Biol. 136, 97–112.
Fincham, J.E., Markus, M.B., Adams, V.J., 2003. Could control of soiltransmitted helminthic infection influence the HIV/AIDS pandemic? Acta Trop. 86, 315–333.
Grando, S.A., Horton, R.M., Pereira, E.F., Diethelm-Okita, B.M., George, P.M., Albuquerque, E.X., Conti-Fine, B.M., 1995. A nicotinic acetylcholine receptor regulating cell adhesion and motility is expressed in human keratinocytes. J. Invest. Dermatol. 105, 774–781.
Grando, S.A., Kist, D.A., Qi, M., Dahl, M.V., 1993. Human keratinocytes synthesize, secrete, and degrade acetylcholine. J. Invest. Dermatol. 101, 32–36.
Hu, Y., Platzer, E.G., Bellier, A., Aroian, R.V., 2010. Discovery of a highly synergistic anthelmintic combination that shows mutual hypersusceptibility. Proc. Natl. Acad. Sci. U.S.A. 107, 5955–5960.
Hu, Y., Miller, M., Zhang, B., Nguyen, T.T., Nielsen, M.K., Aroian, R.V., 2018. In vivo and in vitro studies of Cry5B and nicotinic acetylcholine receptor agonist anthelmintics reveal a powerful and unique combination therapy against intestinal nematode parasites. PLoS Neglected Trop. Dis. 12 (5), e0006506. https://doi.org/10.1371/journal.pntd.0006506.
Kimber, M.J., Sayegh, L., El-Shehabi, F., Song, C., Zamanian, M., Woods, D.J., Day, T.A., Ribeiro, P., 2009. Identification of an Ascaris G protein-coupled acetylcholine receptor with atypical muscarinic pharmacology. Int. J. Parasitol. 39 (11), 1215–1222.
Le Hesran, J.Y., Akiana, J., Ndiaye el, H.M., Dia, M., Senghor, P., Konate, L., 2004. Severe malaria attack is associated with high prevalence of *Ascaris lumbricoides* infection among children in rural Senegal. Trans. R. Soc. Trop. Med. Hyg. 98, 397–399.
Lee, D.L., 1962. The distribution of esterase enzymes in Ascaris lumbricoides. Parasitology 52, 241–260.
Li, B.W., Rush, A.C., Weil, G.J., 2015. Expression of five acetylcholine receptor subunit genes in Brugia malayi adult worms. Int. J. Parasitol. Drugs Drug Resis. 5, 100–109.
Liu, Y., Beyer, A., Aebersold, R., 2016. On the dependency of cellular protein levels on mRNA abundance. Cell 165, 535–550.
Macklin, K.D., Maus, A.D., Pereira, E.F., Albuquerque, E.X., Conti-Fine, B.M., 1998. Human vascular endothelial cells express functional nicotinic acetylcholine receptors. J. Pharmacol. Exp. Therapeut. 287, 435–439.
Martin, R.J., 1993. Neuromuscular transmission in nematode parasites and antinematodal drug action. Pharmacol. Ther. 58, 13–50.
Martin, R.J., Robertson, A.P., 2010. Control of nematode parasites with agents acting on neuro-musculature systems: lessons for neuropeptide ligand discovery. Adv. Exp. Med. Biol. 692, 138–154.
Martin, R.J., Robertson, A.P., 2007. Mode of action of Levamisole and pyrantel anthelmintic resistance, E153 and Q57. Parasitology 134, 1093–1104.
Maus, A.D., Pereira, E.F., Karachunski, P.I., Horton, R.M., Navaneetham, D., Macklin, K., Cortes, W.S., Albuquerque, E.X., Conti-Fine, B.M., 1998. Human and rodent bronchial epithelial cells express functional nicotinic acetylcholine receptors. Mol. Pharmacol. 54, 779–788.
McGhee, J.D., Sleumer, M.C., Bilenky, M., Wong, K., McKay, S.J., Goszczynski, B., Tian, H., Krich, N.D., Khattra, J., Holt, R.A., Baillie, D.L., Kohara, Y., Marra, M.A., Jones, S.J., Moerman, D.G., Robertson, A.G., 2007. The ELT-2 GATA-factor and the global regulation of transcription in the *C. elegans* intestine. Dev. Biol. 302, 627–645.
Mellanby, H., 1955. The identification and estimation of acetylcholine in three parasitic nematodes *Ascaris lumbricoides, Litomosoides carinii*, and the microfilariae of *Dirofilaria repens*. Parasitology 45, 287–294.
Nehrke, K., 2003. A reduction in intestinal cell pHi due to loss of the *Caenorhabditis elegans* Na+/H+ exchanger NHX-2 increases life span. J. Biol. Chem. 278, 44657–44666.
Nejsum, P., Parker, E.D., Frydenburg, J., Sorensen, U.B., Roepstorff, A., Boes, J., Haque, R., Astrup, I., Prag, J., Skov Sørensen, U.B., 2005. Ascariasis is a zoonosis in Denmark. J. Clin. Microbiol. 43, 1142–1148.
Park, B.J., Lee, D.G., Yu, J.R., Jung, S.K., Choi, K., Lee, J., Kim, Y.S., Lee, J.I., Kwon, J.Y., Lee, J., Singson, A., Song, W.K., Eom, S.H., Park, C.S., Kim, D.H., Bandyopadhyay, J., Ahnn, J., 2001. Calreticulin, a calcium-binding molecular chaperone, is required for stress response and fertility in Caenorhabditis elegans. Mol. Biol. Cell 12, 2835–2845.
Peng, D., Wan, D., Cheng, C., Ye, X., Sun, M., 2018. Nematode-specific cadherin CDH-8 acts as a receptor for Cry5B toxin in *Caenorhabditis elegans*. Appl. Microbiol. Biotechnol. 102, 3663–3673.
Prichard, R.K., 1994. Anthelmintic resistance. Vet. Parasiotol. 54, 259–268.
Puttachary, S., Trailovic, S.M., Robertson, A.P., Thompson, D.P., Woods, D.J., Martin, R.J., 2013. Derquantel and Abamectin: effects and interactions on isolated tissues of Ascaris suum. Mol. Biochem. Parasitol. 188, 79–86.
Qian, H., Martin, R.J., Robertson, A.P., 2006. Pharmacology of N-, L-, and B-subtypes of nematode nAChR resolved at the single-channel level in Ascaris suum. Faseb. J. 20, 2606–2608.
Rosa, B.A., Jasmer, D.P., Mitreva, M., 2014. Genome-wide tissue-specific gene expression, co-expression and regulation of co-expressed genes in adult nematode Ascaris suum. PLoS Neglected Trop. Dis. 8 (2), e2678. https://doi.org/10.1371/journal.pntd.0002678.
Rosa, B.A., Townsend, R., Jasmer, D.P., Mitreva, M., 2015. Functional and phylogenetic characterization of proteins detected in various nematode intestinal compartments. Mol. Cell. Proteomics 14, 812–827.
Schulenburg, H., Kurz, C.L., Ewbank, J.J., 2004. Evolution of the innate immune system: the worm perspective. Immunol. Rev. 198, 36–58.
Sloniecka, M., Le Roux, S., Boman, P., Bystrom, B., Zhou, Q., Danielson, P., 2015. Expression profiles of neuropeptides, neurotransmitters, and their receptors in human keratocytes *in vitro* and *in situ*. PloS One 10 (7) 10.1371.
Takahashi, T., Shiraishi, A., Murata, J., 2018. The coordinated activities of nAChR and wnt signaling regilate intestinal stem cell function in mice. Int. J. Mol. Sci. 19, 738. https://doi.org/10.3390/ijms19030738.
Unwin, N., 1993. Nicotinic acetylcholine receptor at 9Å resolution. J. Mol. Biol. 229, 1101–1124.
Urban Jr., J.F., Hu, Y., Miller, M.M., Scheib, U., You, Y.Y., Aroian, R.V., 2013. Bacillus thurgeiensis-derived Cry5B has potent anthelmintic activity against *Ascaris suum*. PLoS Neglected Trop. Dis. 7, e2263. https://doi.org/10.1371/journal.pntd.0002263.
Verma, S., Kaskyap, S., Robertson, A.P., Martin, R.J., 2017. Functional genomics in Brugia malayi reveal diverse muscle nAChRs and differences between cholinergic anthelmintics. Proc. Natl. Acad. Sci. Unit. States Am. 114, 5539–5544.
Wang, F., Flanagan, J., Su, N., Wang, L.C., Bui, S., Nielson, A., Wu, X., Vo, H.T., Ma, X.J.,

Luo, Y., 2012. RNAscope: a novel in situ RNA analysis platform for formalin fixed, paraffin-embedded tissues. J. Mol. Diagn. 14, 22–29.
Wang, Y., Pereira, E.F., Maus, A.D., Ostlie, N.S., Navaneetham, D., Lei, S., Albuquerque, E.X., Conti-Fine, B.M., 2001. Human bronchial epithelial and endothelial cells express alpha7 nicotinic acetylcholine receptors. Mol. Pharmacol. 60, 1201–1209.
WHO, 2017. Soil-transmitted Helminth Infections. World Health Organization Available: http://www.who.int/mediacentre/factsheets/fs366/en/.
Williamson, S.M., Robertson, A.P., Brown, L., Williams, T., Woods, D.J., Martin, R.J., Sattelle, D.B., Wolstenholme, A.J., 2009. The nicotinic acetylcholine receptors of the parasitic nematode Ascaris suum: formation of two distinct drug targets by varying the relative expression levels of two subunits. PLoS Pathog. 5, e1000517. https://doi.org/10.1371/journal.ppat.1000517.
Yin, Y., Martin, J., Abubucker, S., Scott, A.L., McCarter, J.P., Wilson, R.K., Jasmer, D.P., Mitreva, M., 2008. Intestinal transcriptomes of nematodes: comparison of the parasites *Ascaris suum* and *Haemonchus contortus* with the free-living Caenorhabditis elegans. PLoS Neglected Trop. Dis. 2 (8), e269. https://doi.org/10.1371/journal.pntd.0000269.